Wave–Vortex Interactions in Fluids and Superfluids

Oliver Bühler

Courant Institute of Mathematical Sciences, New York University, New York, New York 10012; email: obuhler@cims.nyu.edu

Annu. Rev. Fluid Mech. 2010. 42:205–28

The *Annual Review of Fluid Mechanics* is online at fluid.annualreviews.org

This article's doi:
10.1146/annurev.fluid.010908.165251

0066-4189/10/0115-0205$20.00

Key Words

circulation theorem, Lagrangian-mean theory, pseudomomentum, wave-driven circulation, nonlinear Schrödinger equation

Abstract

This article reviews the methods of wave–mean interaction theory for classical fluid dynamics, and for geophysical fluid dynamics in particular, providing a few examples for illustration. It attempts to bring the relevant equations into their simplest possible form, which highlights the organizing role of the circulation theorem in the theory. This is juxtaposed with a simple account of superfluid dynamics and the attendant wave–vortex interactions as they arise in the nonlinear Schrödinger equation. Here the fundamental physical situation is more complex than in the geophysical case, and the current mathematical understanding is more tentative. Classical interaction theory might be put to good use in the theoretical and numerical study of quantum fluid dynamics.

1. INTRODUCTION

The study of interactions between waves and vortices has a long history in classical fluid dynamics, and especially in geophysical fluid dynamics (GFD), which is concerned with atmosphere and ocean fluid dynamics. This is because of the pressing need in GFD to understand and to model unresolved wave motions in the large-scale numerical models used for climate and weather prediction. The methods of wave–mean interaction theory that have been developed to answer this need are now in a mature state and are described in recent GFD textbooks (McWilliams 2006, Salmon 1998b, Vallis 2006), as well as in dedicated monographs (Bühler 2009). It is therefore timely to draw some of the theoretical threads together and to review the key interaction mechanisms with a few examples, along with a snapshot of how these interaction mechanisms affect the large-scale circulation of the atmosphere.

Another area in which wave–vortex interactions are important is that of superfluidity in quantum fluid dynamics, where quantized line vortices interact, with wave motions representing elementary excitations of the quantum fluid (e.g., Donnelly 1991, Pethick & Smith 2002). In this area much experimental progress has recently been made on Bose-Einstein condensates, which has in turn stimulated renewed theoretical and numerical efforts to model superfluidity. Here we briefly review the fluid dynamics of the mathematically most precisely defined of such models, namely the nonlinear Schrödinger equation. It may be fair to say that there has been little exchange between the fields of geophysical and quantum fluid dynamics, but it seems to me that both fields could benefit from each other's advances, and it is in this spirit that this brief review is offered.

2. WAVE–VORTEX INTERACTIONS IN CLASSICAL FLUIDS

At its core, the study of wave–vortex interactions in classical fluid dynamics is a study of Kelvin's circulation theorem (KCT) and its ramifications. More specifically, by combining the circulation theorem with Lagrangian, particle-following averaging for the flow, it is possible to bring the relevant interaction equations into their simplest form. This is certainly true for the traditional wave–mean interaction results, which are based on spatially periodic waves relative to a basic flow that is symmetric with respect to the periodic coordinate. Interestingly, it turns out also to be true for the more recently studied interactions that do not rely on such global symmetries.

2.1. Kelvin's Circulation Theorem

We start with the compressible Euler equations for perfect fluid flow in the form

$$\frac{D\boldsymbol{u}}{Dt} + \frac{\nabla p}{\rho} = -\nabla\Phi, \tag{1}$$

$$\frac{D\rho}{Dt} + \rho\nabla\cdot\boldsymbol{u} = 0, \quad \text{and} \quad \frac{Ds}{Dt} = 0. \tag{2}$$

Here $\boldsymbol{u} = (u, v, w)$ is the fluid velocity, p is the pressure, ρ is the density, Φ is an external potential such as gravity, and s is the specific entropy per unit mass, which is materially invariant because of the assumption of perfect fluid flow. We assume that an equation of state allows the pressure to be computed as a function of ρ and s, as would be the case for an ideal gas. This ignores moisture effects in the atmosphere and salinity effects in the ocean.

The circulation is defined by the line integral

$$\Gamma = \oint_C \boldsymbol{u}\cdot\boldsymbol{dx}, \tag{3}$$

where $\mathcal{C}$ is a closed material loop, i.e., a closed curve that moves with the fluid. It follows that (e.g., Batchelor 1967)

$$\frac{d\Gamma}{dt} = -\oint_{\mathcal{C}} \frac{\nabla p}{\rho} \cdot \boldsymbol{dx} = -\oint_{\mathcal{C}} \frac{dp}{\rho}. \tag{4}$$

KCT spells out the conditions under which the integral in Equation 4 is zero, which results in the Lagrangian conservation law

$$\text{Kelvin's circulation theorem:} \quad \frac{d\Gamma}{dt} = 0. \tag{5}$$

This is the most interesting formula in fluid dynamics. The condition under which Equation 5 holds is that dp/ρ restricted to $\mathcal{C}$ must be a perfect differential. In the simplest case of incompressible homogeneous flow, ρ is a global constant and Equation 5 holds for any $\mathcal{C}$. The same is true for barotropic flow, in which ρ is a function of p only. An example of this is the flow of an ideal gas with uniform entropy s. Finally, Equation 5 also holds if ρ is a function of both p and s, provided that $\mathcal{C}$ lies within an isentrope, i.e., within a surface of constant s. In this case, the s dependence of ρ plays no role in the integral, and, crucially, if $\mathcal{C}$ lies within an isentrope at the initial time, then it continues to do so at subsequent times by Equation 2b. Notably, the validity of the circulation theorem depends only on the flow on $\mathcal{C}$ itself; i.e., it is not necessary to consider the flow inside the area enclosed by $\mathcal{C}$.

In the stably stratified flows that are relevant to GFD, the entropy increases with altitude, and surfaces of constant s then mark out quasi-horizontal stratification surfaces. It is easy for fluid to flow tangentially along these quasi-horizontal stratification surfaces, but there is a large potential energy cost associated with vertical deformations of these stratification surfaces. The linear waves associated with the restoring mechanism due to this energy cost are the internal gravity waves familiar in GFD (e.g., Salmon 1998b, Vallis 2006).

2.2. Circulation Theorem for the Lagrangian-Mean Flow

Eulerian wave–mean interaction theory is based on a linear averaging operator $\overline{(\ldots)}$ that decomposes any flow field ϕ into a mean part $\bar{\phi}$ and a disturbance part ϕ' such that

$$\phi = \bar{\phi} + \phi' \quad \text{and} \quad \overline{\phi'} = 0 \tag{6}$$

both hold. The second requirement makes sure that averaging is a projection in the sense that $\bar{\bar{\phi}} = \bar{\phi}$. The actual definition of the averaging operator can vary greatly from case to case; for the abstract theory, it is usually easiest to think of an ensemble average, or of an average over a very fast timescale. In practice, the most commonly used averaging operations are zonal averaging, i.e., averaging along latitude circles in the atmosphere and time averaging in the ocean. In either case, the resulting equations for the Eulerian-mean flow are all variants of the Reynolds-averaged equations familiar from the classical theory of incompressible turbulence.

Now, it is well-known that the Eulerian-mean flow $\bar{\boldsymbol{u}}$ does not inherit a version of the circulation theorem (Equation 5), essentially because the Lagrangian information contained in following the material circuit $\mathcal{C}$ is lost under Eulerian averaging. At the price of some additional complexity, this can be remedied in the generalized Lagrangian-mean theory (GLM) of Andrews & McIntyre (1978a,b). Here an additional particle displacement field $\boldsymbol{\xi}(\boldsymbol{x}, t)$ is introduced such that the lifting map

$$\boldsymbol{x} \to \boldsymbol{x} + \boldsymbol{\xi}(\boldsymbol{x}, t) \tag{7}$$

produces the actual position of the particle whose mean position at time t is $\boldsymbol{x}$. It then follows that $\boldsymbol{\xi}$ is a disturbance field, i.e., $\bar{\boldsymbol{\xi}} = 0$. Here the averaging operation is any of the Eulerian averaging

operations discussed above; this makes GLM theory a hybrid Eulerian-Lagrangian theory. With the aid of $\boldsymbol{\xi}$, it is possible to define a Lagrangian-mean velocity field as

$$\bar{\boldsymbol{u}}^L(\boldsymbol{x}, t) = \overline{\boldsymbol{u}(\boldsymbol{x} + \boldsymbol{\xi}(\boldsymbol{x}, t), t)}. \tag{8}$$

The pedantic notation emphasizes that $\boldsymbol{\xi}$ is always evaluated at $(\boldsymbol{x}, t)$. In analogy with Equation 6, one can also define a Lagrangian-disturbance velocity $\boldsymbol{u}^\ell$ via

$$\boldsymbol{u}(\boldsymbol{x} + \boldsymbol{\xi}(\boldsymbol{x}, t), t) = \bar{\boldsymbol{u}}^L(\boldsymbol{x}, t) + \boldsymbol{u}^\ell(\boldsymbol{x}, t) \quad \text{and} \quad \overline{\boldsymbol{u}^\ell} = 0. \tag{9}$$

By construction, the Lagrangian-mean velocity $\bar{\boldsymbol{u}}^L$ is formed by an average over a fixed set of particles, whereas the Eulerian-mean velocity $\bar{\boldsymbol{u}}$ is formed by an average over a fixed set of points. Consequently,

$$\frac{Ds}{Dt} = 0 \Rightarrow \bar{\mathrm{D}}^L \bar{s}^L = 0, \quad \text{where} \quad \bar{\mathrm{D}}^L = \frac{\partial}{\partial t} + \bar{\boldsymbol{u}}^L \cdot \boldsymbol{\nabla} \tag{10}$$

is the derivative following the Lagrangian-mean flow. This can be contrasted with the corresponding Eulerian-mean relation

$$\left(\frac{\partial}{\partial t} + \bar{\boldsymbol{u}} \cdot \boldsymbol{\nabla}\right) \bar{s} = -\overline{\boldsymbol{u}' \cdot \boldsymbol{\nabla} s'}. \tag{11}$$

Clearly, the material advection of s is inherited by $\bar{s}^L$ but not by $\bar{s}$.

Moreover, it can be shown (Andrews & McIntyre 1978a) that Equations 3 and 5 have the exact Lagrangian-mean counterpart

$$\frac{d}{dt} \oint_{\mathcal{C}} (\bar{\boldsymbol{u}}^L - \mathbf{p}) \cdot d\boldsymbol{x} = 0. \tag{12}$$

Here $\mathcal{C}$ is a closed loop that moves with $\bar{\boldsymbol{u}}^L$, and $\mathbf{p}$ is the pseudomomentum vector whose Cartesian components are defined by

$$p_i = -\sum_{k=1}^{3} \overline{\frac{\partial \xi_k}{\partial x_i} u_k^\ell}. \tag{13}$$

The mean circulation theorem (Equation 12) holds under the natural Lagrangian-mean versions of the original conditions. In particular, in the stratified case, Equation 12 holds if $\mathcal{C}$ lies within a surface of constant Lagrangian-mean entropy $\bar{s}^L$.

The mean circulation theorem (Equation 12) can be used to investigate wave–vortex interactions by encircling a vortex with a suitable contour $\mathcal{C}$ either in two dimensions or on a stratification surface in three dimensions. More specifically, we can envisage a steady axisymmetric vortex in the absence of waves, and it is then convenient to make the undisturbed contour axisymmetric as well. To make matters as simple as possible, we can then consider a periodic wave disturbance in the azimuthal direction and use a local tangent-plane approximation in which the undisturbed contour is straightened out to lie along the x axis, for example. We can then use zonal averaging over the periodic x coordinate, and it follows that all mean quantities are independent of x. Under zonal averaging, the mean contour $\mathcal{C}$ remains flat and parallel to the x axis even though the actual material contour traced out by the lifting map (Equation 7) if $\boldsymbol{x} \in \mathcal{C}$ is undulating in a three-dimensional wavelike fashion.

It follows that Equation 12 only involves the zonal, x components of $\bar{\boldsymbol{u}}^L$ and $\mathbf{p}$. Indeed, we have the exact result (Andrews & McIntyre 1978a)

$$\bar{\mathrm{D}}^L \bar{u}^L = \bar{\mathrm{D}}^L \mathrm{p}. \tag{14}$$

This remarkable formula implies that the zonal Lagrangian-mean flow follows the zonal pseudomomentum associated with the wave field. For instance, the formula implies that the vortex is weakened by the waves if the zonal pseudomomentum is retrograde relative to the rotation of the

vortex (i.e., if the sign of p is opposite to the sign of the vortex circulation). This will in fact usually be the case for vortex edge waves, so Equation 14 quantifies the often-observed phenomenon that the disturbance of a vortex edge goes hand in hand with a weakening of the circumferential velocity of the vortex.

Overall, this simple yet exact formula, and its extensions to forced-dissipative flows and to flows in a rotating reference frame, underpins most of the wave–mean interaction theory that is in practical use in atmospheric science. It is possible to derive similar formulas based on an Eulerian definition of a zonal pseudomomentum, but this works only for small wave amplitudes and requires nontrivial modifications in a rotating frame (e.g., Andrews et al. 1987). Eulerian and Lagrangian definitions of p are compared and discussed by Bühler (2009).

2.3. Pseudomomentum of Linear Plane Waves

The pseudomomentum vector $\mathbf{p}$ defined in Equation 13 has a simple generic form in the case of linear plane waves. This generic form is most useful for asymptotic studies of a slowly varying wave train. In particular, if the linear waves are propagating on a constant basic state with velocity $\boldsymbol{U}$, then it is easy to show that

$$\boldsymbol{\xi}_t + (\boldsymbol{U}\cdot\boldsymbol{\nabla})\boldsymbol{\xi} = \boldsymbol{u}' \quad \text{and} \quad \boldsymbol{u}^\ell = \boldsymbol{u}' \tag{15}$$

to first order in the small wave amplitude $a \ll 1$, for example. In a plane wave, all fields are proportional to $\exp(i[\boldsymbol{k}\cdot\boldsymbol{x} - \omega t])$ for some wave-number vector $\boldsymbol{k}$ and frequency ω. Hence Equation 13 becomes (taking real parts as necessary)

$$\mathbf{p} = \frac{\boldsymbol{k}}{\hat{\omega}}\overline{|\boldsymbol{u}'|^2} \tag{16}$$

to $O(a^2)$. Here

$$\hat{\omega} = \omega - \boldsymbol{U}\cdot\boldsymbol{k} \tag{17}$$

is the intrinsic frequency, which differs from the absolute frequency ω by the Doppler-shifting term $\boldsymbol{U}\cdot\boldsymbol{k}$. Under the assumption of equipartition of wave energy between its kinetic and potential forms, this equation can be rewritten in the generic form

$$\mathbf{p} = \frac{\boldsymbol{k}}{\hat{\omega}}\bar{E}, \tag{18}$$

where $\bar{E} \geq 0$ is the mean wave energy per unit mass. Despite the specifics of this derivation, this generic expression in fact holds for all kinds of waves, even those that do not obey the equipartition of energy. This includes sound waves, internal gravity waves with or without Coriolis forces, and even Rossby waves.

Clearly, the sign of the zonal component p is equal to the sign of the intrinsic zonal phase velocity. In other words, one can deduce the sign of p and therefore the sign of the mean-flow response in Equation 14 from the zonal direction of phase propagation relative to the basic flow. For example, in the case of Rossby waves, this intrinsic zonal phase propagation is always retrograde relative to the rotation of Earth, implying that the zonal mean-flow response to Rossby waves is always retrograde as well: A growing Rossby wave goes hand in hand with a westward acceleration of the zonal mean flow.

For internal gravity waves, conversely, either sign is possible for p. In the particular case of steady mountain lee waves caused by a zonal wind U blowing over sinusoidal topography, the intrinsic frequency $\hat{\omega}$ follows from $\omega = 0$ and Equation 17 as

$$\hat{\omega} = -Uk \Rightarrow \mathrm{sgn}(\mathrm{p}) = -\mathrm{sgn}(U). \tag{19}$$

Here k is the zonal wave number of the topography. Here the zonal pseudomomentum is always of opposite sign to the zonal wind causing the waves, in which case Equation 14 implies that the zonal wind is reduced in magnitude at $O(a^2)$ by a growing wave field. For instance, if the wind started to blow over topography at $z = 0$ at time $t = 0$, then the developing internal wave field will have reached up to a finite altitude $Z(t)$ at a later time t; in the simplest scenario, $Z(t)$ grows with the vertical group velocity of the waves. In the region $z > Z$, there are no waves yet, and the zonal flow is at its basic value. However, the region $z < Z$ contains waves, and in there the zonal flow has been weakened by the pseudomomentum at $O(a^2)$. The concomitant momentum change of the zonal flow per unit time as $Z(t)$ grows is equal and opposite to the zonal drag exerted on the mountain below.

As mentioned above, the plane-wave relation (Equation 18) retains its validity in the asymptotic regime of slowly varying wave trains. This is particularly important for the propagation of waves through shear flows, in which the basic velocity $\boldsymbol{U}$ depends on position. In this case, conservation of wave action (Bretherton & Garrett 1968) implies that $\bar{E}/\hat{\omega}$ satisfies a conservation law of the form

$$\frac{\partial}{\partial t}\left(\frac{\bar{E}}{\hat{\omega}}\right) + \boldsymbol{\nabla}\cdot\left(\frac{\bar{E}}{\hat{\omega}}\boldsymbol{c}_g\right) = 0, \tag{20}$$

where $\boldsymbol{c}_g$ is the absolute group velocity, which is the sum of the basic flow $\boldsymbol{U}$ and the intrinsic group velocity $\partial\hat{\omega}/\partial k$ that can be computed from the dispersion relation. In the context of a zonally symmetric basic state, the zonal wave number k is constant following a group-velocity ray, and therefore p inherits the conservation law of wave action; i.e., it follows that

$$\frac{\partial \mathrm{p}}{\partial t} + \boldsymbol{\nabla}\cdot(\mathrm{p}\boldsymbol{c}_g) = 0. \tag{21}$$

It is noteworthy that it is possible to derive an exact conservation law for zonal pseudomomentum p based solely on the zonal symmetry of the mean flow, and that such a conservation law then retains its validity even if wave action is not conserved (e.g., Andrews & McIntyre 1978b, Bühler 2009, Shaw & Shepherd 2008). In this more general case, the flux of zonal pseudomomentum in the meridional, yz plane is known traditionally as the Eliassen-Palm flux. This flux has a simple generic expression in GLM theory but not in Eulerian-mean theory (e.g., Bühler 2009).

We note in passing that in the case of finite-amplitude waves, GLM theory remains formally valid, but that the occurrence of $\boldsymbol{\xi}$ makes it hard to evaluate $\mathbf{p}$ or its flux from observational or computational data. Alternative Eulerian methods to define wave activity measures that are conserved if a suitable reference flow has a corresponding space-time symmetry have been developed using the powerful methods of Hamiltonian fluid mechanics (e.g., Morrison 1998; Salmon 1988a,b; Shaw & Shepherd 2008; Shepherd 1990). These are the methods of choice to diagnose wave dynamics from data, but their utility is restricted to this diagnostic activity. For example, it is usually not possible to link the definition of Eulerian pseudomomentum based on these methods to the evolution of the actual zonal mean flow. Thus Eulerian techniques based on Hamiltonian fluid mechanics and the Lagrangian techniques of GLM theory are complementary in their applicability to wave diagnostics and wave–mean interaction theory.

2.4. Dissipation and the Pseudomomentum Rule

The mean-flow changes described by Equation 14 are bounded by the size of p, which is necessarily small for small-amplitude waves. Larger mean-flow changes can accrue if continuous forcing and dissipation of the waves are brought into play. Specifically, if wave dissipation by a momentum-conserving mechanism such as viscous diffusion is added to the governing equation, then

Equation 14 is replaced by

$$\bar{\mathrm{D}}^L \bar{u}^L = \bar{D}^L \mathrm{p} - \mathcal{F}, \tag{22}$$

where $\mathcal{F}$ quantifies the dissipation of zonal pseudomomentum. [Here, the term momentum-conserving means that if a dissipative force $\boldsymbol{F}$ is added to the right-hand side of Equation 1, then it must be of the form $\boldsymbol{F} = (\boldsymbol{\nabla} \cdot \boldsymbol{T})/\rho$, where $\boldsymbol{T}$ is a stress tensor.] For example, in a situation with linear dissipation, a typical expression for this quantity is $\mathcal{F} = -\alpha p$ with some damping rate per unit time $\alpha > 0$. The best way to understand Equation 22 is by considering a thought experiment in which a spatially compact wave packet propagates without dissipation until at some moment the wave packet is dissipated instantaneously by a suitable $\mathcal{F}$. As the wave packet enters a previously undisturbed region, the zonal mean flow $\bar{\boldsymbol{u}}^L$ first responds in accordance with Equation 14, as described above. When the instantaneous dissipation occurs, the right-hand side of Equation 22 contains two large term terms that cancel each other. In other words, the dissipation destroys the wave packet, but it does not, by itself, accelerate the mean flow (Bühler 2000, 2009; Bühler & McIntyre 2005).

We can extend this thought experiment to a sequence of wave packets all undergoing the same life cycle. It is then clear that the net changes of $\bar{u}^L$ in the dissipation region are cumulative and point in the same direction as p. In the limit of a steady wave train, the time-dependent term on the right-hand side of Equation 22 is zero, and the region of mean-flow acceleration then coincides with the region of wave dissipation. This often-studied case of a steady wave train with dissipation gives rise to the pseudomomentum rule, which is the notion that the mean flow feels the presence of the waves only where and when the waves are dissipating, and that in this case the effective force felt by the zonal mean flow is equal to (minus) the dissipation rate of the zonal pseudomomentum. This is a useful rule in practice, although the thought experiment just described makes clear that wave dissipation only makes permanent mean-flow changes that have already occurred previously due to wave transience.

Essentially the same construction for the dissipative pseudomomentum rule can also be achieved for a three-dimensional packet of internal waves that intersects a given stratification surface. Here zonal averaging is replaced by the usual asymptotic averaging over the rapidly varying phase of the wave packet. This is illustrated in **Figure 1**, which shows a wave packet intersecting a quasi-horizontal stratification surface. At the core of the wave packet, the wave-induced mean flow is forward, i.e., in the direction of $\mathbf{p}_H$. This is as could be expected from Equation 14. In addition, the wave packet is surrounded by a large-scale $O(a^2)$ dipolar return flow, which was first computed by Bretherton (1969). This return flow is peculiar to localized wave packets, and it has no counterpart in the zonal-mean theory that led to Equation 14. If the wave packet dissipates, then the mean flow does not change, but a dipolar pattern of equal-and-opposite vertical vorticity arises as indicated in **Figure 1*b*** (Bühler 2000, McIntyre & Norton 1990). More accurately, the dipolar pattern arises in the distribution of Rossby-Ertel potential vorticity (PV) on the stratification surface under consideration. For example, in the case of Equations 1 and 2, the PV is defined as

$$q = \frac{(\boldsymbol{\nabla} \times \boldsymbol{u}) \cdot \boldsymbol{\nabla} s}{\rho}, \quad \text{with the property that} \quad \frac{Dq}{Dt} = 0 \tag{23}$$

in perfect flow without dissipation. As the wave packet dissipates, a dipolar PV pattern is generated as if a horizontal force equal to (minus) the dissipation rate of horizontal pseudomomentum were acting on the mean flow. As above, the dissipation can only make permanent the mean-flow change that arose from wave transience. Notably, this dissipation pattern implies that the horizontal pseudomomentum of the wave packet reappears as the horizontal impulse of the PV distribution. This is an instance of a more general conservation law that is discussed in Section 2.6 below.

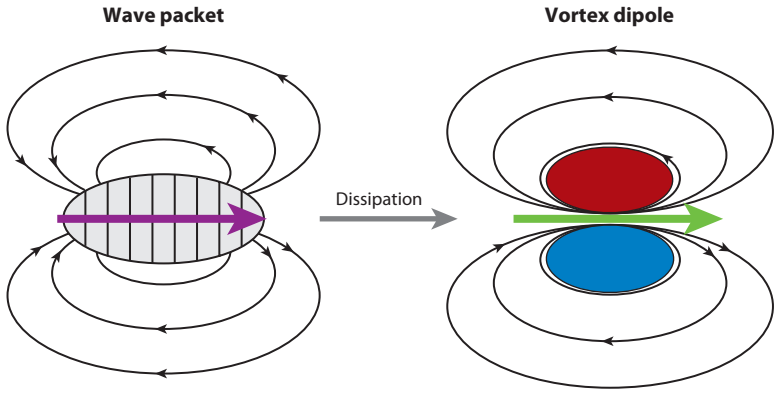

Figure 1

View from above of a three-dimensional packet of internal waves that intersects a horizontal stratification surface. The large-scale $O(a^2)$ return flow is indicated by the black lines. As the wave packet dissipates, it turns into a vortex dipole. The purple arrow indicates both the direction of propagation of the wave packet and the horizontal pseudomomentum vector $\mathbf{p}_H$ according to Equation 14. The horizontal pseudomomentum of the wave packet before dissipation equals the horizontal impulse of the potential-vorticity distribution after dissipation.

2.5. The Wave-Driven Circulation in the Middle Atmosphere

In the long run, the persistent forcing due to dissipating waves that is felt by the zonally averaged zonal mean flow according to Equation 22 can lead to a significant large-scale flow response in the atmosphere, especially in the middle atmosphere, which lies between approximately 20 and 80 km in altitude. The main component missing in Equation 22 is Earth's rapid rotation. Basically, on a rotating planet, the zonal accelerations due to a zonally symmetric prograde (i.e., eastward) force give rise to Coriolis forces that push the air equatorward, toward the region of higher absolute angular momentum. Conversely, a retrograde (i.e., westward) force leads to Coriolis forces that push the air poleward. This is true in both hemispheres.

By mass conservation, the poleward or equatorward push due to the Coriolis forces leads to a global-scale zonal-mean circulation in the meridional, latitude-altitude plane. This gyroscopic pumping effect of the wave-induced zonal forces is illustrated in **Figure 2**. In the lower and middle stratosphere, the retrograde force due to Rossby waves dominates, leading to the Brewer-Dobson circulation, which is an equator-to-pole circulation in both hemispheres with corresponding upwelling in the equatorial region and downwelling over the poles.

The prevailing zonal winds in the summer hemisphere do not allow topographically forced Rossby or gravity waves to propagate higher up into the mesosphere, but it is possible for prograde gravity waves to make this journey, and this leads to an effective prograde force in the summer mesosphere (e.g., Andrews et al. 1987, Bühler & McIntyre 1999, Bühler et al. 1999). Conversely, there is no such lack of retrograde Rossby waves in the winter hemisphere, and this leads to a retrograde force in the winter mesosphere. Combining these force patterns therefore leads to the Murgatroyd-Singleton circulation, which is circulation from summer pole to winter pole, with upwelling over the summer pole and downwelling over the winter pole. The adiabatic cooling associated with the expansion of air parcels in the rising branch of this circulation over the summer pole is responsible for the peculiar fact that the summer polar mesophere is both the sunniest place on Earth and also the coldest, with observed temperatures as low as −163°C (McIntyre 2003).

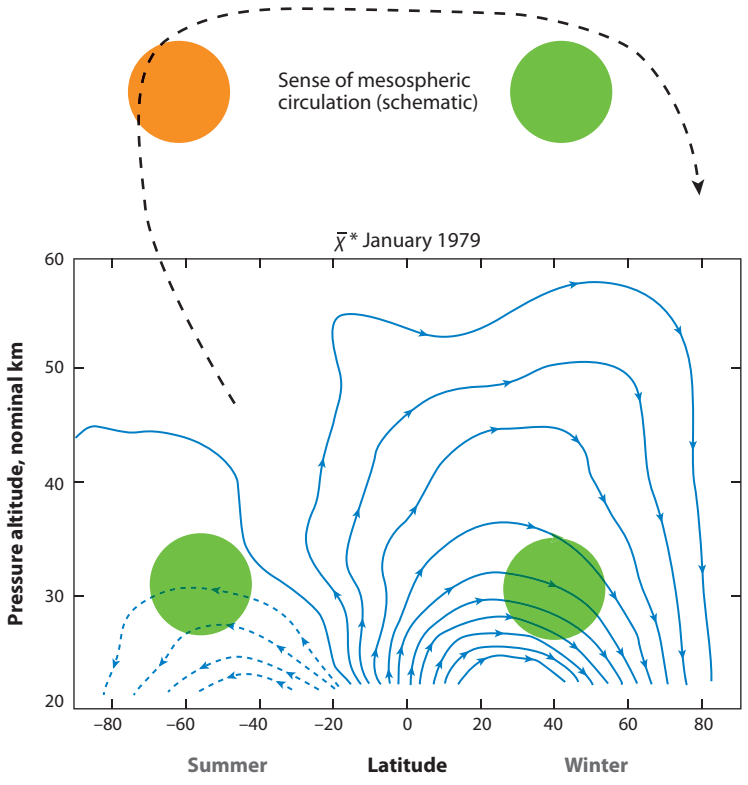

Figure 2

Mass-transport streamlines, indicating the wave-driven meridional circulation in the middle atmosphere. Retrograde wave-induced forces due to Rossby waves and gravity waves are displayed in green, and prograde forces due to gravity waves are displayed in orange.

These examples illustrate the importance of the wave-induced transport of angular momentum for the global-scale circulation of the atmosphere; further examples and more theoretical detail of how the meridional circulation at some altitude depends on effective forces higher up are discussed comprehensively by Haynes et al. (1991). The global conservation of angular momentum is crucial to achieve the right physical results here, and this is also important for the design of numerical models, which need to take this angular-momentum constraint into account (e.g., Shepherd & Shaw 2004).

2.6. Conservation Law for Pseudomomentum Plus Impulse

The classical interaction theory discussed in the previous section excludes effects regarding the three-dimensional refraction of waves by vortices. This matters for localized wave–vortex interactions, in which both the waves and the relevant mean flow depend on all spatial coordinates. Recent wave-vortex refraction studies involving internal gravity waves include Plougonven & Snyder (2005), Hasha et al. (2008) in atmospheric science, Polzin (2008) in oceanography, and Snyder et al. (2007) in idealized GFD.

Refraction is most easily studied in the regime of slowly varying linear waves, in which the general methods of ray tracing together with the conservation of wave action readily deliver

the solution. A simple system for illustration is the two-dimensional shallow-water system. The governing equations are

$$\frac{D\boldsymbol{u}}{Dt} + g\boldsymbol{\nabla} h = 0 \quad \text{and} \quad \frac{Dh}{Dt} + h\boldsymbol{\nabla}\cdot\boldsymbol{u} = 0. \tag{24}$$

Here $\boldsymbol{u} = (u, v)$ is the horizontal velocity, h is the layer depth, and g is gravity. The fields $(\boldsymbol{u}, h)$ depend on the horizontal coordinates $\boldsymbol{x} = (x, y)$ and time t. The relevant PV is

$$q = \frac{\boldsymbol{\nabla}\times\boldsymbol{u}}{h} = \frac{v_x - u_y}{h}, \quad \text{which has the property} \quad \frac{Dq}{Dt} = 0. \tag{25}$$

We assume an $O(1)$ vortical flow with slowly varying velocity field $\boldsymbol{U}(\boldsymbol{x}, t)$. If the Froude number based on $\boldsymbol{U}$ is sufficiently low, then we can neglect $O(1)$ variations of the layer depth; i.e., we can treat the $O(1)$ layer depth H as constant.

A slowly varying wave train with central wave-number vector $\boldsymbol{k}(\boldsymbol{x}, t)$ containing shallow-water surface waves is then governed by the dispersion relation

$$\omega = \hat{\omega}(\boldsymbol{k}) + \boldsymbol{U}\cdot\boldsymbol{k} \quad \text{with} \quad \hat{\omega}(\boldsymbol{k}) = \sqrt{gH}|\boldsymbol{k}|. \tag{26}$$

The absolute group velocity is

$$\boldsymbol{c}_g = \sqrt{gH}\frac{\boldsymbol{k}}{|\boldsymbol{k}|} + \boldsymbol{U}, \quad \text{and} \quad \frac{d}{dt} = \frac{\partial}{\partial t} + \boldsymbol{c}_g\cdot\boldsymbol{\nabla} \tag{27}$$

is the time-derivative along a ray. The wave-action conservation law takes the generic form of Equation 20. The evolution of $\boldsymbol{k}$ along a ray is then given by

$$\frac{d\boldsymbol{k}}{dt} = -(\boldsymbol{\nabla}\boldsymbol{U})\cdot\boldsymbol{k} \Leftrightarrow \frac{dk_i}{dt} = -\sum_{k=1}^{2}\frac{\partial U_k}{\partial x_i}k_k. \tag{28}$$

For example, in the case of a zonally symmetric mean flow, the zonal component of $\boldsymbol{k}$ would remain constant along a ray. In combination with Equation 20, this would then lead to the integral conservation of zonal pseudomomentum, as discussed above. In the more general case, this is no longer true, and hence no component of $\mathbf{p}$ is conserved. Indeed, combining Equations 20 and 28 leads to

$$\frac{\partial\mathbf{p}}{\partial t} + \boldsymbol{\nabla}\cdot(\mathbf{p}\boldsymbol{c}_g) = -(\boldsymbol{\nabla}\boldsymbol{U})\cdot\mathbf{p}. \tag{29}$$

This shows that the pseudomomentum is refracted in the same way as the wave-number vector. Assuming a compact wave field, a domain-integrated form of Equation 29 is

$$\boldsymbol{\mathcal{P}} = \int \mathbf{p}\,dxdy \quad \text{and} \quad \frac{d\boldsymbol{\mathcal{P}}}{dt} = -\int(\boldsymbol{\nabla}\boldsymbol{U})\cdot\mathbf{p}\,dxdy. \tag{30}$$

The changes in $\mathbf{p}$ or $\boldsymbol{\mathcal{P}}$ due to refraction raise the question as to how the basic flow $\boldsymbol{U}$ is itself affected. In other words, is there a generalization of Equation 14 that allows for local refraction?

If the velocity field $\boldsymbol{U}$ is induced by vortices, then a simple conservation law exists that regulates the interplay of the pseudomomentum and the impulse of the mean vorticity distribution (Bühler & McIntyre 2005). To demonstrate this, we use the Lagrangian-mean versions of Equation 25 (Bühler & McIntyre 1998):

$$\bar{q}^L = \frac{\boldsymbol{\nabla}\times(\bar{\boldsymbol{u}}^L - \mathbf{p})}{\tilde{h}} \quad \text{and} \quad \bar{D}^L\bar{q}^L = 0. \tag{31}$$

Here $\tilde{h}$ is defined by

$$\bar{\mathrm{D}}^L\tilde{h} + \tilde{h}\boldsymbol{\nabla}\cdot\bar{\boldsymbol{u}}^L = 0. \tag{32}$$

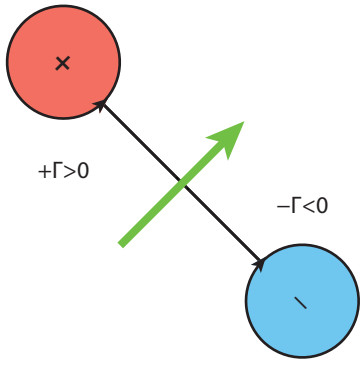

Figure 3

Impulse of a vortex couple consisting of two vortices with equal-and-opposite circulations $\pm\Gamma$. The impulse vector points in the direction of propagation of the couple and has magnitude $|\boldsymbol{\mathcal{I}}| = \Gamma R$, where R is the distance between the vortices. Notice that the couple speed is proportional to Γ/R, whereas its two-dimensional vortex interaction energy is proportional to $\Gamma^2 \ln R$. Hence, with decreasing R, the impulse and the energy of the couple both decrease, but its speed increases.

The impulse based on $\bar{q}^L$ is

$$\boldsymbol{\mathcal{I}} = \int (-y, +x)\tilde{h}\bar{q}^L \, dxdy = \int (-y, +x)\boldsymbol{\nabla} \times (\bar{\boldsymbol{u}}^L - \mathbf{p})dxdy. \tag{33}$$

As an example, the impulse of a vortex couple is depicted in **Figure 3**. It is well-known that the impulse of a two-dimensional or three-dimensional vorticity field in incompressible fluid dynamics has a number of attractive properties. For instance, in an unbounded domain, the impulse is conserved. Moreover, the impulse integral does not suffer from the well-known ambiguity of the momentum integral, which is not absolutely convergent in an unbounded domain, even for compact vortical structures such as vortex rings or vortex couples in two dimensions (e.g., Lamb 1932, Theodorsen 1941). Impulse theory has also been used to measure fluid-body interaction forces in studies of animal locomotion (e.g., Bühler 2007, Dabiri 2009, Drucker & Lauder 1999). It is therefore quite a natural idea to use impulse theory for wave–vortex interactions.

The time derivative of $\boldsymbol{\mathcal{I}}$ is easily evaluated by applying $\bar{\mathrm{D}}^L$ to the entire integrand, including $dxdy$. Both $\bar{q}^L$ and $\tilde{h}dxdy$ are mean material invariants, and hence the only nonzero term comes from $\bar{\mathrm{D}}^L(y, -x) = (\bar{v}^L, -\bar{u}^L)$. After some integration by parts, this yields

$$\frac{d\boldsymbol{\mathcal{I}}}{dt} = \int (\bar{\boldsymbol{u}}^L - \mathbf{p})\boldsymbol{\nabla} \cdot \bar{\boldsymbol{u}}^L \, dxdy + \int (\boldsymbol{\nabla}\bar{\boldsymbol{u}}^L) \cdot \mathbf{p} \, dxdy \tag{34}$$

up to a remainder that vanishes in an unbounded domain if $\bar{q}^L$ and $\mathbf{p}$ are compact (Bühler 2009, Bühler & McIntyre 2005). In the last term, $\mathbf{p}$ contracts with $\bar{\boldsymbol{u}}^L$ and not with $\boldsymbol{\nabla}$. So far we have used exact GLM theory for $\boldsymbol{\mathcal{I}}$, but now we ignore the $\boldsymbol{\nabla} \cdot \bar{\boldsymbol{u}}^L$ term under the assumption of low Froude number for the mean flow. Comparing Equations 30 and 34 then yields

$$\frac{d(\boldsymbol{\mathcal{P}} + \boldsymbol{\mathcal{I}})}{dt} = 0, \tag{35}$$

which is the sought-after conservation law for the sum of pseudomomentum and impulse. Notably, Equation 35 also remains valid in the presence of momentum-conserving dissipation, which makes clear that in **Figure 1** the net pseudomomentum of the wave packet before dissipation is equal to the impulse of the vortex couple after dissipation.

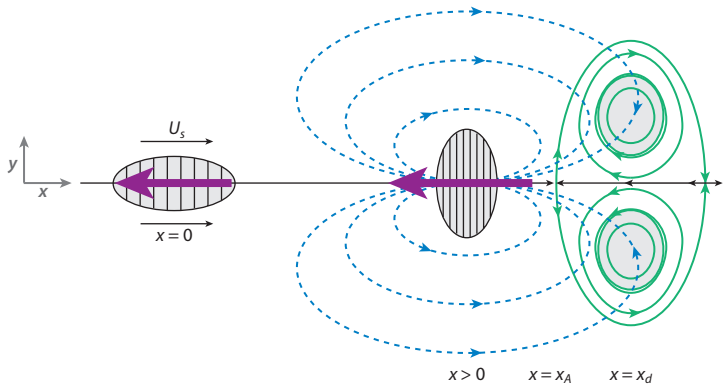

Figure 4

Two snapshots of a wave packet undergoing refraction due to the strain flow induced by the vortex couple on the right. The flow is viewed in a reference frame moving with the vortex couple, and the induced strain is such that it compresses the wave packet in the x direction, which increases $|k|$ and therefore increases $|\mathcal{P}|$. The conservation law (Equation 35) makes clear that there must be a concomitant decrease of the impulse $|\mathcal{I}|$, which is confirmed by detailed calculation: The large-scale Bretherton return flow of the wave packet (indicated by the *stippled lines*) pushes the vortex couple closer together and thereby lowers its impulse by the right amount. Figure taken from Bühler & McIntyre 2005.

The conservation law for $\mathcal{I} + \mathcal{P}$ makes it easier to analyze wave–vortex interactions involving refraction. For example, **Figure 4** illustrates a wave packet undergoing refraction. The gain in the wave packet's pseudomomentum is balanced by a loss in the couple's impulse. It is apparent that this kind of nonlocal action-at-distance interaction between waves and vortices is quite different from the standard wave–mean interactions (such as Equation 14) that occur in the theory of zonally symmetric mean flows.

Overall, the material reviewed above shows how the interplay between the circulation theorem, the Lagrangian-mean flow, and the pseudomomentum regulates the wave–vortex interactions in classical fluid dynamics. We now turn to quantum fluid dynamics, in which we note similarities with the classical wave–vortex interactions.

3. SUPERFLUIDS

Superfluidity is a macroscopic quantum effect that can arise at very low temperatures in certain materials. Outstanding among a remarkable score of unusual fluid-dynamical behavior exhibited by superfluids is the possibility of quantized vortex lines (e.g., Donnelly 1991, 1993). The classic example of superfluid material is liquid helium II, which exhibits superfluidity below a temperature T of approximately 2.17 K. More recently (since 1995), the production of dilute Bose-Einstein condensates by laser cooling in laboratory experiments has provided an example of superfluidity in which quantized vortex lines are directly observable (e.g., Pethick & Smith 2002). This has greatly stimulated renewed interest in superfluid dynamics, and even in superfluid turbulence (e.g., Barenghi et al. 2001).

The traditional reference point for a continuum description of superfluidity at low-but-finite temperature is the two-fluid model of Landau, in which the fluid is conceived as an inseparable mixture of two interpenetrating components termed the super and the normal components (e.g., Landau & Lifshitz 1959). The super component executes inviscid irrotational flow (including quantized vortex lines) and carries zero entropy. In contrast, the normal component executes

standard viscous flow and carries all the fluid entropy. The two fluids are not independent, but are coupled dynamically through various force terms, describing effects such as mutual friction. Their relative abundance is temperature dependent such that the normal component is absent at $T = 0$ and the super component is absent at the transition temperature.

Apart from requiring a certain suspension of disbelief on behalf of classical fluid dynamicists, the two-fluid model (and its various extensions over the years that account more fully for quantized vortex lines) suffers from the presence of a large number of adjustable constants in the model, and from a certain ambiguity of the exact terms that should appear in the equations. Arguably, these problems effectively prohibit a comprehensive fundamental mathematical and computational study of the two-fluid model.

An attractive alternative in this regard is the study of superfluidity using the dynamics of a macroscopic wave function for the particle locations, which leads to the nonlinear Schrödinger (NLS) equation. This appears to be a faithful model of superfluidity of dilute systems at very low temperatures, and it naturally includes quantized vortex lines, as well as elementary wave excitations that can interact with these vortices. Indeed, it is broadly agreed that such wave excitations are a model for the normal component in the two-fluid model, and sometimes it is even speculated that a full thermodynamic ensemble of such waves would recover the two-fluid model in its entirety (e.g., Sonin 2001).

We now provide a simple account of the fluid dynamics described by the NLS equation, and then discuss wave–vortex interactions. Whenever possible, we compare results with the classical results reviewed above. Of course, the basics of quantum fluid dynamics are readily available elsewhere, but it is convenient for discussion to assemble all the pieces in one place.

3.1. The Nonlinear Schrödinger Equation

The NLS equation, also called the Gross-Pitaevskii equation, is a model equation for the collective wave function that governs the behavior of a condensate of N identical bosons near absolute zero temperature $T = 0$. Formally, the equation is derived under two assumptions. First, the N-particle wave function Ψ of quantum mechanics is approximated by a product of N identical copies of the single-particle wave function $\tilde{\psi}$, i.e.,

$$\Psi(\boldsymbol{x}_1, \boldsymbol{x}_2, \ldots, \boldsymbol{x}_N, t) = \prod_{i=1}^{N} \tilde{\psi}(x_i, t). \tag{36}$$

Here the particle locations $\boldsymbol{x}_i \in \mathcal{D} \subset \mathbb{R}^3$ live in some bounded domain $\mathcal{D}$, for example. The product form in Equation 36 implies that the particles are independent, and we also have the normalizations

$$\int_{\mathcal{D}} |\Psi|^2 dV_1 \ldots dV_N = 1 \quad \text{and} \quad \int_{\mathcal{D}} |\tilde{\psi}|^2 dV = 1. \tag{37}$$

Second, the pair interactions between any two particles are approximated by a potential energy function V, given by

$$V(\boldsymbol{x}_i, \boldsymbol{x}_j) = U_0 \boldsymbol{\delta}(\boldsymbol{x}_i - x_j) \quad \text{for} \quad i \neq j. \tag{38}$$

Here $U_0 > 0$ is a constant, and Equation 38 provides the simplest possible model for the repulsive short-range interactions between two particles. [It is not possible to derive a precise value for U_0 from microscopic theory, but a typical expression is $U_0 = 4\pi\hbar a^2/m$, where a is the particle radius and m is its mass (Pethick & Smith 2002).] The expected energy of the N particles then follows

from the usual Hamiltonian operator of quantum mechanics as

$$N\int_{\mathcal{D}}\left(\frac{\hbar^2}{2m}|\nabla\tilde{\psi}|^2+V(\boldsymbol{x})|\tilde{\psi}|^2+\frac{N-1}{2}U_0|\tilde{\psi}|^4\right)dV. \tag{39}$$

Here $\hbar$ is Planck's constant divided by 2π, m is the mass of a particle, and $V(\boldsymbol{x})$ is an external potential that might be present. There are $N(N-1)/2$ pair interaction terms, and they multiply the wave function raised to the fourth power.

The form of Equation 39 suggests the use of a scaled wave function

$$\psi(\boldsymbol{x},t)=\sqrt{N}\tilde{\psi}(\boldsymbol{x},t)\quad\text{such that}\quad\int_{\mathcal{D}}|\psi|^2dV=N, \tag{40}$$

and therefore for $N\gg 1$, the expected energy takes the simpler form

$$\int_{\mathcal{D}}\left(\frac{\hbar^2}{2m}|\nabla\psi|^2+V(\boldsymbol{x})|\psi|^2+\frac{1}{2}U_0|\psi|^4\right)dV. \tag{41}$$

For stationary states, this expression can be used to determine the ground-level energy states by minimization under the particle-conservation constraint (Equation 40) (e.g., Pethick & Smith 2002). Conversely, a time-dependent evolution equation for $\psi(\boldsymbol{x},t)$ can be derived by applying the standard methods of Hamiltonian mechanics for continuous fields to the expected energy functional (Equation 41). If $U_0=0$, this yields the usual linear Schrödinger equation, and if $U_0\neq 0$ it yields the NLS equation

$$i\,\hbar\psi_t=-\frac{\hbar^2}{2m}\nabla^2\psi+[V(\boldsymbol{x})+U_0|\psi|^2]\psi. \tag{42}$$

The boundary conditions are $\psi=0$ on $\boldsymbol{x}\in\partial\mathcal{D}$. Notably, the nonlinearity in Equation 42 appears in undifferentiated form via the magnitude of ψ, showing that in low-density regions, the NLS equation is well approximated locally by the linear Schrödinger equation. This is much simpler than the nonlinearity in Equation 1. Also, Equation 42 can be simply integrated numerically using an operator-splitting method, which again contrasts with the classical compressible fluid equations.

3.2. The Madelung Transformation and Vortices

The NLS equation can be made intelligible to fluid dynamicists via the celebrated Madelung transformation, which is based on the polar representation of ψ in the form

$$\psi=\sqrt{n}\exp(i\theta), \tag{43}$$

where $n(\boldsymbol{x},t)\geq 0$ and $\theta(\boldsymbol{x},t)$ are real-valued functions describing the expected particle density and the wave phase, respectively. Clearly,

$$n(\boldsymbol{x},t)=|\psi(\boldsymbol{x},t)|^2, \tag{44}$$

and therefore $n(\boldsymbol{x},t)$ satisfies the continuity equation

$$n_t+\nabla\cdot\boldsymbol{j}=0, \tag{45}$$

where the usual probability current vector

$$\boldsymbol{j}=-\frac{i\hbar}{2m}(\psi^*\nabla\psi-\psi\nabla\psi^*)=+\frac{\hbar}{m}\Im(\psi^*\nabla\psi)=\frac{\hbar}{m}n\nabla\theta. \tag{46}$$

This motivates the definition of a velocity vector $\boldsymbol{u}(\boldsymbol{x},t)=\boldsymbol{j}/n$ for the condensate via

$$\boldsymbol{u}=\frac{\hbar}{m}\nabla\theta=\frac{\hbar}{m}\frac{\Im(\psi^*\nabla\psi)}{|\psi|^2}. \tag{47}$$

If ψ is replaced by its complex conjugate ψ^*, then $\boldsymbol{u}$ changes its sign. This is a simple manifestation of the time reversibility of the NLS equation; i.e., replacing an initial condition of the NLS equation by its complex conjugate reverses the direction of time.

The continuity equation then takes the standard form

$$n_t + \boldsymbol{\nabla} \cdot (n\boldsymbol{u}) = 0 \Leftrightarrow \frac{Dn}{Dt} + n\boldsymbol{\nabla} \cdot \boldsymbol{u} = 0, \tag{48}$$

which is familiar from Equation 2a with ρ replaced by n. The definition of $\boldsymbol{u}$ as the gradient of θ makes clear that

$$\boldsymbol{\nabla} \times \boldsymbol{u} = 0 \tag{49}$$

holds, albeit only in a weak sense. Specifically, Equation 49 holds at any point at which $\psi \neq 0$, but it can be violated at zeros of ψ, which correspond to vortices. The velocity field is singular at such vortex locations, and the right-hand side of Equation 49 then acquires a delta function centered at the vortex location. A simple kinematic example in two dimensions is the following. We let

$$\psi = x + iy = r\exp(i\alpha) \Rightarrow n = r^2 \quad \text{and} \quad \theta = \alpha, \tag{50}$$

where (r, α) are cylindrical coordinates such that $x = r\cos\alpha$ and $y = r\sin\alpha$. Hence θ is multiple valued,

$$\boldsymbol{u} = \frac{\hbar}{m}\frac{(-y, +x)}{x^2 + y^2}, \tag{51}$$

and the circulation of $\boldsymbol{u}$ around any closed contour $\mathcal{C}$ enclosing the origin is

$$\Gamma = \oint_{\mathcal{C}} \boldsymbol{u} \cdot \boldsymbol{dx} = 2\pi\frac{\hbar}{m}. \tag{52}$$

This is the celebrated occurrence of quantized vortex lines in superfluids, which correspond to zero lines of the complex wave function ψ. [Higher-order vortices with circulations that are integer multiples of $2\pi\hbar/m$ are also possible; e.g., $\psi = (x+iy)^2$ has circulation $4\pi\hbar/m$. However, such higher-order vortices play a limited role in practice because they are likely to split into several first-order vortices with the same net circulation.] Notably, the occurrence of such zero lines in three dimensions (and the occurrence of zero points in two dimensions) is generic for a complex function such as ψ, because such a line is the intersection of the zero surfaces of the real and imaginary parts of ψ.

At first sight, it may seem that a single vortex such as Equation 50 may spontaneously appear or disappear in the course of the time-dependent dynamics of the NLS equation, but this is not the case. Indeed, an isolated vortex can neither appear nor disappear at all under NLS dynamics. Essentially, this is because around the vortex the phase of ψ increases by 2π, and this topological fact cannot be undone by the differential dynamics of the NLS equation. A direct proof of the same fact follows from KCT once we have written down the governing equations for θ and $\boldsymbol{u}$, which follow from Equation 42 after the substitution of Equation 43. This leads to

$$\frac{\hbar}{m}\theta_t + \frac{|\boldsymbol{u}|^2}{2} + \frac{1}{m}[V(\boldsymbol{x}) + U_0 n] - \frac{\hbar^2}{2m^2}\frac{\nabla^2\sqrt{n}}{\sqrt{n}} = 0. \tag{53}$$

The occurrence of $1/\sqrt{n}$ signals that this equation is well defined away from zeros of ψ, i.e., away from vortex locations. Similarly, away from vortex locations, the gradient of Equation 53 gives

$$\frac{D\boldsymbol{u}}{Dt} + \boldsymbol{\nabla}\left\{\frac{1}{m}[V(\boldsymbol{x}) + U_0 n] - \frac{\hbar^2}{2m^2}\frac{\nabla^2\sqrt{n}}{\sqrt{n}}\right\} = 0, \tag{54}$$

where Equation 49 has been used in the vector identity $(\boldsymbol{u}\cdot\boldsymbol{\nabla})\boldsymbol{u} = \frac{1}{2}\boldsymbol{\nabla}|\boldsymbol{u}|^2 + (\boldsymbol{\nabla}\times\boldsymbol{u})\times\boldsymbol{u}$. Remarkably, the $U_0 n$ term stemming from the repulsive interactions is the same as the pressure-gradient term

in shallow water (Equation 24) or in polytropic flow with the ratio of specific heats equal to two. In other words, the repulsive nonlinearity in the NLS equation gives rise to an effective pressure that is proportional to the density squared. Conversely, the term $-\hbar^2\nabla^2\sqrt{n}$ resembles the effect of surface tension. Importantly, both terms appear inside the gradient, so KCT holds along material contours $\mathcal{C}$ that do not pass through vortices, where $\boldsymbol{u}$ is singular.

It is easy to compute the structure of a steady point vortex in two dimensions (e.g., Donnelly 1991), and the density n varies from zero at the vortex line to its background value n_0 over a radial distance comparable to the so-called healing length

$$\xi = \frac{\hbar}{\sqrt{2mn_0U_0}}. \tag{55}$$

A simple approximation for the density structure is $n(r) \approx n_0 r^2/(r^2 + \xi^2)$, which shows that Equation 50 is accurate at leading order in the radius r.

Now, we again consider the two-dimensional situation with a single vortex at the origin and put a closed contour $\mathcal{C}$ around the vortex and subsequently move this contour with $\boldsymbol{u}$. Then KCT applies in its simplest form to this material contour, and therefore $\Gamma(\mathcal{C})$ cannot change its value, and a single isolated vortex can neither appear nor disappear in the NLS equation. This conclusion holds even though the vortex need not move with $\boldsymbol{u}$ itself, because if an isolated vortex disappears during some infinitesimal time interval Δt, then it is always possible to find a contour $\mathcal{C}$ that encloses the vortex location at a finite distance during this interval. An analogous conclusion holds in three dimensions: A finite-size vortex ring can only disappear if it shrinks to zero radius (Jones & Roberts 1982).

The persistence of isolated vortices under NLS dynamics raises the question of how such vortices can be generated or destroyed at all. Naturally, interactions of the superfluid with solid walls or with foreign bodies such as ions can lead to vortex generation (e.g., Berloff 2000). More subtly, in two-dimensional flows, for example, it is possible to have the spontaneous pair generation of two equal-and-opposite point vortices that are infinitesimally separated. The generation or destruction of such an infinitesimal dipole does not violate KCT because the velocity field in this case is singular on a material contour that is threaded through the infinitesimal gap between the vortices. An analogous possibility exists for infinitesimal vortex rings in three dimensions.

The spontaneous generation and destruction of infinitesimal vortex dipoles in two dimensions are easily demonstrated using the linear Schrödinger equation, which is a valid local approximation to the NLS equation if $|\psi|^2$ is small enough. Basically, this applies to the local flow structure around vortices within the healing length ξ. Setting both V and U_0 to zero in Equation 42 and rescaling time by $m/\hbar$ lead to

$$\psi_t = \frac{i}{2}\nabla^2\psi. \tag{56}$$

An initial condition that corresponds to two equal-and-opposite vortices at $\boldsymbol{x} = (0, 0)$ and $\boldsymbol{x} = (1, 0)$ is

$$\psi(x, y, 0) = (x + iy)(x - 1 - iy) = x^2 - x + y^2 - iy. \tag{57}$$

This is only a local model for ψ, so we do not worry about the growth of $|\psi|$ with distance. The linear solution to this initial-value problem is

$$\psi(x, y, t) = x^2 - x + y^2 - i(y - 2t). \tag{58}$$

This has zeros at

$$x = \frac{1}{2} \pm \frac{1}{2}\sqrt{1 - 16t^2} \quad \text{and} \quad y = 2t. \tag{59}$$

Clearly, the vortices are moving with speed 2 in the y direction, but they are also getting closer together in the x direction, and at time $t = 1/4$ they collide and disappear.

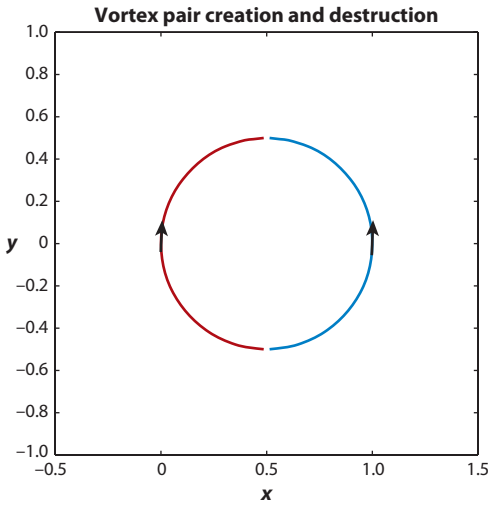

Figure 5

Vortex pair creation and destruction in the solution (Equation 58) to the linear Schrödinger equation. Shown in red and blue are the trajectories of the positive and negative vortex, respectively, and the arrows indicate the direction of propagation. The bending direction of the trajectories is opposite to that suggested by analogy with a classical Magnus force.

Actually, the solution (Equation 58) is also valid for negative times, meaning that the vortices were pair-generated at $(\boldsymbol{x}, t) = (1/2, -1/2, -1/4)$, separated, reached maximum distance at $t = 0$, and then converged again until they disappeared at $t = 1/4$. This life cycle is illustrated in **Figure 5**. Presumably the same construction can be achieved for three-dimensional vortex rings, and there is certainly plentiful numerical evidence for the spontaneous generation of vortex rings (e.g., Berloff & Barenghi 2004).

Despite the ease with which vortices can be identified and manipulated in the Schrödinger equation, it is worth noting that the assumptions that went into the derivation of the NLS equation break down on molecular scales comparable to the interatomic spacing. The healing length ξ is comparable to these molecular scales, and therefore the detailed vortex core structure in the NLS equation is not realistic.

3.3. Vortex Dynamics

A quantum vortex line is a zero line of the complex wave function ψ, so the vortex line is marked by the absence of condensate. Conversely, the velocity $\boldsymbol{u}$ is defined by the continuity equation (Equation 48) for the condensate, so by definition it is the velocity with which the condensate moves. It is therefore not too surprising that there is no fundamental link between the motion of a quantum vortex line and $\boldsymbol{u}$. This is in striking contrast to classical incompressible fluid dynamics, in which vorticity is frozen into the fluid, and hence vortex lines necessarily move as material lines. (If the flow is barotropic, i.e., if the density is a function of pressure only, then the same is also true for the density-scaled vector field $\nabla \times \boldsymbol{u}/\rho$ in classical compressible fluid dynamics.)

The simple vortex pair example in **Figure 5** demonstrates this point. Specifically, by Equation 57, the condensate velocity at $t = 0$ is

$$\boldsymbol{u} = \frac{\boldsymbol{j}}{n} = \frac{(2xy - y, y^2 - x^2 + x)}{(x^2 - x + y^2)^2 + y^2}. \tag{60}$$

At this instant, the left vortex is located at $\boldsymbol{x} = (0, 0)$, and it easy to show that the average of $\boldsymbol{u}$ over a small square centered at the vortex location is equal to (0, 1). In other words, the averaged velocity at the left vortex is equal to the classical induced velocity due to the right vortex, which has circulation $\Gamma = -2\pi$ and is located at $x = (1, 0)$ (cf. Equation 64 below). However, Equation 59 shows that the left vortex moves with velocity (0, 2) at this instant, which is twice the classical induced velocity. This makes unambiguously clear that quantum vortices do not in general move with the condensate velocity.

In the light of this, there has been a considerable effort (discussed in detail in Donnelly 1991 and Barenghi et al. 2001) to find a dynamical equation for the motion of quantum vortex lines that allows the study of interactions between several vortices as well as between vortices and elementary wave excitation such as phonons and rotons (see Section 3.4 below). For example, in two dimensions the motion of a quantum vortex line relative to the condensate is sometimes compared with the motion of a solid cylinder with circulation that moves relative to a classical incompressible fluid. This gives rise to a Magnus force acting on the cylinder to which the cylinder then responds like a single particle endowed with an added mass due to the exterior fluid motion. Specifically, in the classical two-dimensional situation, the Magnus force is

$$\boldsymbol{F} = \rho\Gamma\hat{z} \times \boldsymbol{U}, \tag{61}$$

where ρ is the fluid density, Γ is the circulation around the cylinder, $\hat{z}$ is the vertical unit vector, and $\boldsymbol{U}$ is the motion of the cylinder relative to the ambient fluid. The velocity $\boldsymbol{U}(t)$ then evolves according to

$$(m_c + m_a)\frac{d\boldsymbol{U}}{dt} = \boldsymbol{F} = \rho\Gamma\hat{z} \times \boldsymbol{U}, \tag{62}$$

where $m_c + m_a$ is the mass of the cylinder plus the added mass of the displaced fluid. Working by analogy, an effective Magnus force is therefore sometimes postulated for quantum vortex lines. However, the solid cylinder played an essential role in the classical example because it bears the dipolar pressure load caused by the relative motion of the cylinder with respect to the fluid. It is not obvious that the "soft" compressible core of a quantum vortex can play the role of the solid cylinder. (If the quantum vortex circulation is attached to a wire threading the condensate, as might be the case in some experimental set ups, then the analogy with the classical Magnus force is much better.) That is not to say that the analogy with the classical Magnus force is wrong in all cases, but rather that it is hard to discern the range of validity of this analogy.

For what it is worth, it appears that the bending of the vortex trajectories in **Figure 5** cannot be explained by Magnus forces. Specifically, at $t = 0$ the left vortex (which has positive circulation) moves with speed (0, 2) while the local condensate moves with the average speed (0, 1). Hence the vortex is faster than the condensate, therefore $\boldsymbol{U} = (0, 1)$ in Equation 61, and the Magnus force points to the left. But the depicted vortex trajectory bends to the right, i.e., in the opposite direction to that suggested by the Magnus force in Equation 62.

Conversely, a point vortex in two dimensions can indeed be simply advected by a slowly varying condensate velocity. Essentially this already follows from the Galilean invariance of the linear Schrödinger equation. For example, if the single-vortex initial condition (Equation 50) is replaced by

$$\psi(x, y, 0) = e^{iyV}(x + iy), \quad \text{then} \quad \psi(x, y, t) = e^{iyV - iV^2t/2}[x + i(y - Vt)]. \tag{63}$$

Here the unitary factor $\exp(iyV)$ adds a constant velocity field $(0, V)$ that is a simple model for a slowly varying velocity field, and Equation 63 makes clear that the vortex is simply advected by this velocity. This contrasts with Equation 57, where the factor $x - 1 - iy$ corresponds to a

velocity field near the origin equal to $(0, 1) + (y, x) + O(r^2)$. This is not slowly varying compared to the vortex core, which is $O(1)$ in this example.

This gives rise to the classical approximation to quantum vortex dynamics, which is based on two assumptions: first, that the density n is approximately equal to its background value n_0 everywhere outside the vortex cores, and second, that the vortices are well separated in the sense that their separation r satisfies $r \gg \xi$. The first assumption is reasonable for small velocities and large-scale flows, because in this case the nonlinear term in the NLS equation ensures that there are only weak density fluctuations, and hence $n \approx n_0$ and $\nabla \cdot \boldsymbol{u} \approx 0$ outside the vortex cores. The second assumption can be controlled for the initial conditions, but there is no guarantee that the dynamical evolution of the quantum state will maintain this assumption.

In two dimensions, this means that a vortex at (x_1, y_1) with circulation Γ_1 induces the classical velocity field

$$\boldsymbol{u} = \frac{\Gamma_1}{2\pi} \frac{[-(y - y_1), +(x - x_1)]}{(x - x_1)^2 + (y - y_1)^2} \tag{64}$$

at distances large compared to ξ. Therefore, M well-separated vortices with positions $(x_i, y_i) \in \mathbb{R}^2$ and circulations Γ_i move according to the classical Hamiltonian set of ordinary differential equations first proposed by Kirchhoff (Lamb 1932):

$$\Gamma_i \frac{dx_i}{dt} = +\frac{\partial H}{\partial y_i} \quad \text{and} \quad \Gamma_i \frac{dy_i}{dt} = -\frac{\partial H}{\partial x_i}, \tag{65}$$

where the Hamiltonian function is

$$H(x_1, y_1, \ldots, x_M, y_M) = -\frac{1}{2\pi} \sum_{j=2}^{M} \sum_{i=1}^{j-1} \Gamma_i \Gamma_j \ln r_{ij} \tag{66}$$

in terms of the vortex separations $r_{ij} = |\boldsymbol{x}_i - \boldsymbol{x}_j|$. This dynamical system preserves the value of H as well as the impulse vector

$$\mathcal{I} = \sum_{i}^{M} (-y_i, +x_i)\Gamma_i \tag{67}$$

and the angular momentum

$$J = \sum_{i}^{M} (x_i^2 + y_i^2)\Gamma_i. \tag{68}$$

The partial analogy with classical point vortex dynamics also extends to bounded flows. For example, if a quantum vortex is far away from a straight impermeable wall, then the effect of the wall on the vortex is well represented by the usual image vortex construction (Mason et al. 2006). This is not completely obvious because the quantum boundary condition is $\psi = 0$ at a wall, whereas the classical condition is $\boldsymbol{u} \cdot \boldsymbol{n} = 0$ in terms of the unit vector normal to the wall. However, just as in the vortex core, the density adjusts from zero to its background value over a short distance away from the wall that is comparable to the healing length ξ. In other words, the direct impact of the quantum boundary condition is confined to a thin boundary layer, and there can be no probability current into this boundary layer, so $\boldsymbol{u} \cdot \boldsymbol{n} = 0$ applies at a short distance normal to the wall.

The validity of Equation 65 for well-separated quantum vortices makes available the well-known results of classical point vortex dynamics. It also makes available the statistical mechanics methods that have been developed for the classical situation (e.g., Bühler 2002). Of course, if two vortices get too close to each other (or if one vortex gets too close to a wall), then Equation 65 loses its validity, the vortices do not move according to classical theory anymore, and we also face the possibility of spontaneous pair creation or destruction.

3.4. Linear Wave Spectrum

The linear wave spectrum of the NLS equation for small perturbations relative to a uniform basic state with $n = n_0$ and $\boldsymbol{u} = 0$ is easily computed. For plane-wave perturbations of the form $\exp(i[\boldsymbol{k}\cdot\boldsymbol{x} - \omega t])$ with wave-number vector $\boldsymbol{k}$ and frequency ω, one obtains the dispersion relation

$$\omega^2 = c^2\kappa^2 + \frac{\hbar^2}{4m^2}\kappa^4 \quad \text{where} \quad \kappa = |k| \quad \text{and} \quad c^2 = \frac{n_0 U_0}{m}. \tag{69}$$

Thus for small wave numbers, there is the nondispersive sound wave regime $\omega^2 = c^2\kappa^2$, whereas for higher wave numbers, the dispersive κ^4 term comes into play. Compared with classical fluid dynamics in two dimensions, this dispersion relation is identical to that of the shallow-water equations with surface tension (e.g., Whitham 1974). In quantum mechanics, the low-wave-number excitations described by Equation 69 are called phonons. In general, elementary excitations such as phonons are interpreted as a model for the normal fluid component in the two-fluid model.

The linear wave spectrum has a particularly important interpretation in quantum mechanics because of the proportionality (for plane waves) between the expected momentum and energy of an elementary excitation and the wave-number vector $\boldsymbol{k}$ and the frequency ω, respectively. In other words, in quantum mechanics, a plot of ω as a function of κ is interpreted as a plot of energy E as a function of momentum p, for example. In this interpretation, the low-wave-number part of Equation 69 corresponds to $E \propto p$, a relationship that is familiar from light waves, i.e., photons. Conversely, the large-wave-number part of the spectrum corresponds to $E \propto p^2$, as in the kinetic energy for single particles in classical mechanics.

Despite these appealing interpretations, the actual spectrum of elementary excitations for liquid helium is not well described by Equation 69 for large wave numbers. Indeed, the true spectrum is not monotonic, but rather it dips down and exhibits a conspicuous interior minimum of $E(p)$ at a wavelength comparable with the interatomic spacing. This minimum is particularly important, as it is associated with observable excitations called rotons, but it is clearly not present in the linear plane-wave spectrum of the NLS equation.

It is possible to modify the pair-interaction model (Equation 38) to allow for nonlocal interactions to obtain a better fit between the NLS spectrum and the observed spectrum, although one has to be careful that the implied sign reversal of the group velocity $d\omega/d\kappa$ does not lead to other unwanted dynamical effects, such as unphysical particle clustering (e.g., Berloff & Roberts 2001). However, the available microscopic theories for rotons are not based on plane-wave excitations (Feynman 1956). Indeed, Feynman visualized the molecular dynamics of a roton as the smallest possible vortex ring (or vortex pair in two dimensions) in which individual molecules move forward in a narrow and short channel while there is a large-scale dipolar return flow that surrounds this forward flow and ensures that the probability current is nondivergent. In Feynman's (1998) words, "A roton can be visualized as a group of children going down a slide. After sliding down, the children go around and come back to the slide again." The similarity between this roton image and the wave packet with the Bretherton return flow in **Figure 1** is striking.

3.5. Wave–Vortex Interactions in the Nonlinear Schrödinger Equation

The interactions between quantized vortex lines and wave excitations are the central dynamical topic in NLS theory. We restrict our discussion to the two-dimensional case, in which the vortex lines correspond to point vortices. One fundamental interaction mechanism is the creation of point vortices either in the fluid interior or at a boundary. [As discussed above, the circulation theorem implies that, in the fluid interior, only the pair creation of vortices is possible, but at a boundary (such as a cylinder moving through the fluid), a single-sign vortex may be locally created.] For

smooth flows, a simple scaling argument from classical fluid dynamics then prevails because, to produce a vortex, the fluid density must reach zero. Relative density variations in compressible flows are proportional to the square of the Mach number, or equivalently the Froude number in shallow water, implying that vortex creation requires flow speeds of the order of the nondispersive wave speed c in Equation 69.

Another fundamental interaction mechanism is the scattering of linear plane waves by a point vortex, and the concomitant back-reaction on the vortex that is often referred to as mutual friction. This process is interpreted as a model of the interaction of vortex lines with the normal component of the fluid in the two-fluid model, whereby the propagation of waves past the vortex line is viewed as motion of the normal component relative to the vortex line. Despite the clarity of the linear scattering problem, the situation is mathematically difficult because of the singularity of $\boldsymbol{u}$ at the vortex, which requires careful asymptotic treatment (e.g., Llewellyn Smith 2002). Moreover, cumulative effects accrue only at $O(a^2)$ in the small wave number $a \ll 1$, so in principle this involves nonlinear effects.

For example, in a perturbation expansion where $n = n_0 + an_1 + a^2 n_2 + \ldots$ and the other fields are ordered in powers of $a \ll 1$, the current $n\boldsymbol{u}$ at $O(a^2)$ is often approximated by $n_1\boldsymbol{u}_1$, where n_1 and $\boldsymbol{u}_1$ are the linear solutions. However, this neglects mean-flow response terms such as $n_2\boldsymbol{u}_0$ and $n_0\boldsymbol{u}_2$, which enter at the same order and which are not known from the linear solution. It is well-known from classical fluid dynamics that these mean-flow response terms can be important in wave-mean interaction problems (e.g., Bühler 2009, McIntyre 1981). Presumably, these difficulties are compounded when approximate plane-wave scattering results are superimposed incoherently to obtain an interaction result for a broad spectrum of plane waves (e.g., Nazarenko et al. 1995).

In view of these mathematical complications, it is perhaps not too surprising that a number of different formulas and numerical constant have been proposed by different authors to account for these wave–vortex interactions. For example, there has been ambiguity about the existence and magnitude of the Iordanskii force, which is conceived as a transverse, Magnus-type force at finite temperature associated with the flow of the normal fluid past the vortex line (e.g., Barenghi et al. 2001, Sonin 2001, Stone 2000, Wexler 1997).

The straightforward numerical integration of the NLS equation makes simulation the tool of choice for studying complex wave–vortex interactions. This is particularly true for studies of the nonlinear interplay of many wave modes and many vortices, and for studies of a forced-dissipative state (e.g., Nazarenko & Onorato 2006).

With regard to fundamental wave–vortex interactions, it might be useful to apply GLM theory with its definitions of $\bar{\boldsymbol{u}}^L$ and $\mathbf{p}$ to the NLS equation. For instance, one advantage might be that by construction $\bar{\boldsymbol{u}}^L$ contains the entire mean material fluid motion, so, for example, it combines the irrotational Eulerian-mean flow $\bar{\boldsymbol{u}}$ with the $O(a^2)$ Stokes drift $\bar{\boldsymbol{u}}^S$ due to the waves, which need not be irrotational itself. More specifically, $\boldsymbol{\nabla} \times \bar{\boldsymbol{u}}^L = \boldsymbol{\nabla} \times \bar{\boldsymbol{u}}^S = \boldsymbol{\nabla} \times \mathbf{p}$ holds for irrotational flow (Andrews & McIntyre 1978a), and there is no reason why $\mathbf{p}$ should be irrotational. This might help clarify some of the remaining issues surrounding the mutual-friction computation and the controversy regarding the Iordanskii force.

In addition, the mean circulation theorem described in Section 2.2 remains valid for the NLS equation. This follows easily from the analogy between shallow-water flow with surface tension and the NLS flow outside vortex cores. The mean PV expression (Equation 31) then implies that $\bar{q}^L$ is zero except at vortex locations, where it has a delta function contribution. This means that the impulse $\boldsymbol{\mathcal{I}}$ based on $\bar{q}^L$ has the classical point vortex form (Equation 67).

It seems inevitable that the refraction of phonon waves away from the vortex cores then gives rise to changes in the waves' total pseudomomentum $\mathcal{P}$ that are described by Equation 30. Similarly, the Bretherton return flow indicated in **Figure 1** must be present in the nearly incompressible

NLS dynamics as well, and therefore one can hypothesize that the conservation law (Equation 35) holds for superfluids described by the NLS equations. In other words, the leap-frogging wave–vortex interaction in **Figure 4** is possible in superfluids. It would be tempting to draw conclusions about mutual friction and the Iordanskii force from a combination of this conservation law and a linear scattering calculation, but once again it is not clear how the wave–vortex interactions near the vortex core, where the quantum fluid is compressible, affect the conservation law.

Overall, it seems likely that in the near future a combination of the theoretical methods of wave–mean interaction theory together with careful numerical simulations will resolve the outstanding fundamental dynamical questions about wave–vortex interactions in the NLS system. Of course, this does not mark the end of quantum fluid dynamics or superfluid turbulence, because the NLS system is only an idealized model for the behavior of real quantum fluids close to zero temperature, but it does mark an important milestone on the path toward a self-consistent predictive theory of finite-temperature superfluidity.

DISCLOSURE STATEMENT

The author is not aware of any affiliations, memberships, funding, or financial holdings that might be perceived as affecting the objectivity of this review.

LITERATURE CITED

Andrews DG, Holton JR, Leovy CB. 1987. *Middle Atmosphere Dynamics*. New York: Academic

Andrews DG, McIntyre ME. 1978a. An exact theory of nonlinear waves on a Lagrangian-mean flow. *J. Fluid Mech.* 89:609–46

Andrews DG, McIntyre ME. 1978b. On wave-action and its relatives. *J. Fluid Mech.* 89:647–64

Barenghi C, Donnelly R, Vinen W, eds. 2001. *Quantized Vortex Dynamics and Superfluid Turbulence*. Lect. Notes Phys. vol. 571. New York: Springer

Batchelor GK. 1967. *An Introduction to Fluid Dynamics*. Cambridge, UK: Cambridge Univ. Press

Berloff N. 2000. Vortex nucleation by a moving ion in a bose condensate. *Phys. Lett. A* 277:240–44

Berloff N, Barenghi C. 2004. Vortex nucleation by collapsing bubbles in Bose-Einstein condensates. *Phys. Rev. Lett.* 93:090401

Berloff N, Roberts P. 2001. Vortices in nonlocal condensate models of superfluid helium. In *Quantized Vortex Dynamics and Superfluid Turbulence*, ed. C Barenghi, R Donnelly, W Vinen, pp. 268–75. New York: Springer

Bretherton FP. 1969. On the mean motion induced by internal gravity waves. *J. Fluid Mech.* 36:785–803

Bretherton FP, Garrett CJR. 1968. Wavetrains in inhomogeneous moving media. *Proc. R. Soc. Lond. A* 302:529–54

Bühler O. 2000. On the vorticity transport due to dissipating or breaking waves in shallow-water flow. *J. Fluid Mech.* 407:235–63

Bühler O. 2002. Statistical mechanics of strong and weak point vortices in a cylinder. *Phys. Fluids* 14:2139–49

Bühler O. 2007. Impulsive fluid forcing and water strider locomotion. *J. Fluid Mech.* 573:211–36

Bühler O. 2009. *Waves and Mean Flows*. Cambridge Monogr. Mech. Cambridge, UK: Cambridge Univ. Press

Bühler O, McIntyre ME. 1998. On non-dissipative wave–mean interactions in the atmosphere or oceans. *J. Fluid Mech.* 354:301–43

Bühler O, McIntyre ME. 1999. On shear-generated gravity waves that reach the mesosphere. Part II: wave propagation. *J. Atmos. Sci.* 56:3764–73

Bühler O, McIntyre ME. 2005. Wave capture and wave-vortex duality. *J. Fluid Mech.* 534:67–95

Bühler O, McIntyre ME, Scinocca JF. 1999. On shear-generated gravity waves that reach the mesosphere. Part I: wave generation. *J. Atmos. Sci.* 56:3749–63

Dabiri JO. 2009. Optimal vortex formation as a unifying principle in biological propulsion. *Annu. Rev. Fluid Mech.* 41:17–33

Donnelly RJ. 1991. *Quantized Vortices in Helium II*. Cambridge, UK: Cambridge Univ. Press
Donnelly RJ. 1993. Quantized vortices and turbulence in helium II. *Annu. Rev. Fluid Mech.* 25:325–71
Drucker EG, Lauder GV. 1999. Locomotor forces on a swimming fish: three-dimensional vortex wake dynamics quantified using digital particle image velocimetry. *J. Exp. Biol.* 202:2393–412
Feynman R. 1956. Energy spectrum of the excitations in liquid helium. *Phys. Rev.* 102:1189–204
Feynman RP. 1998. *Statistical Mechanics*. Reading, MA: Addison-Wesley
Hasha AE, Bühler O, Scinocca J. 2008. Gravity-wave refraction by three-dimensionally varying winds and the global transport of angular momentum. *J. Atmos. Sci.* 65:2892–906
Haynes PH, Marks CJ, McIntyre ME, Shepherd TG, Shine KP. 1991. On the "downward control" of extratropical diabatic circulations by eddy-induced mean zonal forces. *J. Atmos. Sci.* 48:651–78
Jones C, Roberts P. 1982. Motions in a Bose condensate, IV. Axisymmetric solitary waves. *J. Phys. A* 15:2599–619
Lamb H. 1932. *Hydrodynamics*. Cambridge, UK: Cambridge Univ. Press. 6th ed.
Landau LD, Lifshitz EM. 1959. *Fluid Mechanics.* New York: Pergamon. 1st Engl. ed.
Llewellyn Smith SG. 2002. Scattering of acoustic waves by a superfluid vortex. *J. Phys. A* 35:3597–607
Mason P, Berloff N, Fetter AL. 2006. Motion of a vortex line near the boundary of a semi-infinite uniform condensate. *Phys. Rev. A* 74:043611
McIntyre ME. 1981. On the 'wave momentum' myth. *J. Fluid Mech.* 106:331–47
McIntyre ME. 1992. Atmospheric dynamics: some fundamentals, with observational implications. In *Proc. Int. School Phys. "Enrico Fermi", CXV Course*, ed. JC Gille, G Visconti, pp. 313–86. Amsterdam: North-Holland
McIntyre Me. 2003. On global-scale atmospheric circulations. In *Perspectives in Fluid Dynamics: A Collective Introduction to Current Research*, ed. GK Batchelor, HK Moffatt, MG Worster, pp. 557–624. Cambridge, UK: Cambridge Univ. Press. 631 pp.
McIntyre ME, Norton WA. 1990. Dissipative wave-mean interactions and the transport of vorticity or potential vorticity. *J. Fluid Mech.* 212:403–35
McWilliams JC. 2006. *Fundamentals of Geophysical Fluid Dynamics*. Cambridge, UK: Cambridge Univ. Press
Morrison PJ. 1998. Hamiltonian description of the ideal fluid. *Rev. Mod. Phys.* 70:467–521
Nazarenko S, Onorato M. 2006. Wave turbulence and vortices in Bose-Einstein condensation. *Phys. D* 219:1–12
Nazarenko SV, Zabusky NJ, Scheidegger T. 1995. Nonlinear sound-vortex interactions in an inviscid isentropic fluid: a two-fluid model. *Phys. Fluids* 7:2407–19
Pethick C, Smith H. 2002. *Bose-Einstein Condensation in Dilute Gases*. Cambridge, UK: Cambridge Univ. Press
Plougonven R, Snyder C. 2005. Gravity waves excited by jets: propagation versus generation. *Geophys. Res. Lett.* 32:L18802
Polzin KL. 2008. Mesoscale eddy–internal wave coupling. I. Symmetry, wave capture and results from the mid-ocean dynamics experiment. *J. Phys. Oceanogr.* 38:2556–74
Salmon R. 1988a. Hamiltonian fluid mechanics. *Annu. Rev. Fluid Mech.* 20:225–56
Salmon R. 1998b. *Lectures on Geophysical Fluid Dynamics*. New York: Oxford Univ. Press
Shaw T, Shepherd T. 2008. Wave-activity conservation laws for the three-dimensional anelastic and Boussinesq equations with a horizontally homogeneous background flow. *J. Fluid Mech.* 594:493–506
Shepherd TG. 1990. Symmetries, conservation laws, and Hamiltonian structure in geophysical fluid dynamics. *Adv. Geophys.* 32:287–338
Shepherd TG, Shaw TA. 2004. The angular momentum constraint on climate sensitivity and downward influence in the middle atmosphere. *J. Atmos. Sci.* 61:2899–908
Snyder C, Muraki D, Plougonven R, Zhang F. 2007. Inertia-gravity waves generated within a dipole vortex. *J. Atmos. Sci.* 64:4417–31
Sonin E. 2001. Magnus force, Aharanov-Bohm effect, and Berry phase in superfluids. In *Quantized Vortex Dynamics and Superfluid Turbulence*, ed. C Barenghi, R Donnelly, W Vinen, pp. 131–37. New York: Springer
Stone M. 2000. Iordanskii force and the gravitational Aharonov-Bohm effect for a moving vortex. *Phys. Rev. B* 61:11780–86

Theodorsen T. 1941. Impulse and momentum in an infinite fluid. In *Von Karman Anniversary Volume*, pp. 49–57. Pasadena, CA: Caltech

Vallis GK. 2006. *Atmospheric and Oceanic Fluid Dynamics: Fundamentals and Large-Scale Circulation*. Cambridge, UK: Cambridge Univ. Press

Wexler C. 1997. Magnus and Iordanskii forces in superuids. *Phys. Rev. Lett.* 79:1321–24

Whitham GB. 1974. *Linear and Nonlinear Waves*. New York: Wiley-Interscience

Annual Review of
Fluid Mechanics

Volume 42, 2010

Contents

Indexes

Errata

An online log of corrections to *Annual Review of Fluid Mechanics* articles may be found at http://fluid.annualreviews.org/errata.shtml